Korean J Physiol Pharmacol 2024;28(1):93-103
https://doi.org/10.4196/kjpp.2024.28.1.93

KJPP

Original Article

Store-operated calcium entry in the satellite glial cells of rat sympathetic ganglia

Sohyun Kim, Seong Jun Kang, Huu Son Nguyen, and Seong-Woo Jeong*

Department of Physiology, Laboratory of Molecular Neurophysiology, Yonsei University Wonju College of Medicine, Wonju 26426, Korea

ARTICLE INFO

Received December 4, 2023
Revised December 15, 2023
Accepted December 17, 2023

***Correspondence**
Seong-Woo Jeong
E-mail: swjeong@yonsei.ac.kr

Key Words
Calcium signaling
Ganglia, sympathetic
Inflammation
Lipopolysaccharide
Satellite glial cell

ABSTRACT Satellite glial cells (SGCs), a major type of glial cell in the autonomic ganglia, closely envelop the cell body and even the synaptic regions of a single neuron with a very narrow gap. This structurally unique organization suggests that autonomic neurons and SGCs may communicate reciprocally. Glial Ca^{2+} signaling is critical for controlling neural activity. Here, for the first time we identified the machinery of store-operated Ca^{2+} entry (SOCE) which is critical for cellular Ca^{2+} homeostasis in rat sympathetic ganglia under normal and pathological states. Quantitative real-time PCR and immunostaining analyses showed that Orai1 and stromal interaction molecules 1 (STIM1) proteins are the primary components of SOCE machinery in the sympathetic ganglia. When the internal Ca^{2+} stores were depleted in the absence of extracellular Ca^{2+}, the number of plasmalemmal Orai1 puncta was increased in neurons and SGCs, suggesting activation of the Ca^{2+} entry channels. Intracellular Ca^{2+} imaging revealed that SOCE was present in SGCs and neurons; however, the magnitude of SOCE was much larger in the SGCs than in the neurons. The SOCE was significantly suppressed by GSK7975A, a selective Orai1 blocker, and Pyr6, a SOCE blocker. Lipopolysaccharide (LPS) upregulated the glial fibrillary acidic protein and Toll-like receptor 4 in the sympathetic ganglia. Importantly, LPS attenuated SOCE *via* downregulating Orai1 and STIM1 expression. In conclusion, sympathetic SGCs functionally express the SOCE machinery, which is indispensable for intracellular Ca^{2+} signaling. The SOCE is highly susceptible to inflammation, which may affect sympathetic neuronal activity and thereby autonomic output.

INTRODUCTION

Satellite glial cells (SGCs) are the predominant glial cell type found in the autonomic ganglia and, closely envelop the cell bodies of postganglionic neurons and cholinergic synaptic regions. This unique structural arrangement implies a functional unit between neurons and SGCs, indicating that reciprocal communication is essential for regulating autonomic ganglia function [1,2]. Recent studies have highlighted that sympathetic SGCs play critical roles in the physiological regulation of neuronal metabolism and survival, cell excitability, synaptic transmission, and overall sympathetic output [3,4]. Previous studies showed that certain pathological conditions including chronic heart failure [5], cirrhosis [6], and traumatic brain injury [7] cause autonomic imbalance due to sympathetic overactivity. However, the involvement of SGCs in the cellular mechanisms underlying abnormal sympathetic output remains largely unexplored.

Glial calcium (Ca^{2+}) signaling is a key mechanism for neuron-glial communication, regulating the release of various gliotransmitters such as ATP, which affects neuronal activity [8,9]. This signaling cascade is activated in response to diverse extracellular stimuli, such as neurotransmitters released by neurons [10]. The primary source of glial Ca^{2+} signaling is Ca^{2+} release from the endoplasmic reticulum (ER) through the activation of the G-pro-

Author contributions: S.W.J. designed the experimental study and wrote the manuscript. S.K. performed the experiments, statistical analysis, and wrote the manuscripts. S.J.K. and H.S.N. assisted with methodology and contributed resources. All authors contributed to the editing of the revised manuscript and approved the manuscript.

tein-coupled receptor/phospholipase C/inositol 1,4,5-triphosphate receptor (IP_3R) cascade. Restoration of intracellular Ca^{2+} stores following receptor-activated ER Ca^{2+} release necessitates store-operated calcium entry (SOCE) [11]. The primary machinery that activates SOCE is the calcium release-activated calcium channel (CRAC), which comprises Orai channels spanning the plasma membrane and stromal interaction molecule (STIM), an ER Ca^{2+} sensor. The depletion of ER Ca^{2+} triggers the oligomerization of STIM1 and STIM2 monomers leading to their translocation near the plasma membrane, where they form distinct puncta with Orai1, Orai2, and Orai3, thereby activating the Orai Ca^{2+} channels [12]. This activation results in a transient increase in cytosolic Ca^{2+} *via* activated Orai Ca^{2+} channels, and subsequent refilling of ER stores occurs through Ca^{2+} pumps on the ER membrane.

While SOCE has been extensively studied in various glial cells within the central nervous system, including astrocytes, oligodendrocytes, microglia, and Muller glia [13-18], information on glial Ca^{2+} signaling and its mechanisms in the autonomic ganglia remains scarce. Evidence suggests that dysregulation of SOCE in astrocytes and microglia occurs under conditions like lipopolysaccharide (LPS)-induced inflammation [17,19]. As an initial exploration into the physiological and pathophysiological roles of glial Ca^{2+} signaling in autonomic ganglia, we examined the presence of SOCE and its machinery in rat superior cervical ganglia (SCG). Additionally, we examined whether LPS treatment affects SOCE in sympathetic SGCs.

METHODS

Experimental animals

All animal care and experimental procedures followed the National Institutes of Health Guidelines for Care and Use of Experimental Animals and were approved by the Institutional Animal Care and Use Committee of Yonsei University, Wonju College of Medicine (Approval No. YWC-181002-1). Six-week-old male Sprague-Dawley rats obtained from DBL Co. were kept under pathogen-free conditions with a 12:12 h light-dark cycle, temperature of 23°C ± 2°C, and *ad libitum* access to food and water.

Preparation of sympathetic neurons-SGC units

To obtain sympathetic neurons attached with SGCs, a pair of SCG were dissected and enzymatically dissociated using some modifications of the previously described methods [20]. Briefly, the ganglia were desheathed, cut into small pieces, and transferred to Earle's balanced salt solution (EBSS, pH 7.4) (Sigma-Aldrich) containing 1.5 mg/ml collagenase type D (Roche), 0.5 mg/ml trypsin (Worthington Co.), and 0.1 mg/ml DNase type I (Sigma-Aldrich) in a 25-cm^2 tissue culture flask. The EBSS was modified by adding 3.6 mg/l glucose, 10 mM HEPES (Sigma-Aldrich), and 1% penicillin-streptomycin (PS) (HyClone). After bubbling with 95% O_2–5% CO_2, the flask was placed in a shaking water bath at 37°C for 45 min. Following incubation, DMEM (Gibco) with 10% fetal bovine serum (HyClone) and 1% PS were added to the flask to inactivate the digestive enzymes. The ganglia were mechanically dispersed into a pool of partially dissociated cells by gentle trituration using a wide-bore fire-polished glass pipette. After centrifugation at 600 rpm for 6 min, dissociated cells were resuspended in DMEM. Then, as described previously [21], the Schwann cells and myelin debris were removed using a cushion of 10% and 5% bovine serum albumin (BSA, Sigma-Aldrich). This step is critical for separating the partially dissociated neurons attached to the SGCs. The cells were subsequently plated on 12-mm cover glasses coated with poly-D-lysine (Sigma-Aldrich) and maintained in a humidified 95% air–5% CO_2 incubator at 37°C until use.

Immunohistochemistry and immunocytochemistry

The animals were deeply anesthetized with isoflurane (Troika) and perfused transcardially with phosphate-buffered saline (PBS) followed by 4% paraformaldehyde (PFA) (GeneAll Biotechnology) in PBS. SCG were harvested, post-fixed in 4% PFA for 6 h at 4°C, and cryoprotected with 30% sucrose in PBS (Sigma-Aldrich) overnight at 4°C. Tissue samples were embedded in the Tissue-Tek OCT compound (Sakura Finetek) in plastic molds and stored at –80°C. Frozen tissues were sectioned at 7 μm thickness on a crytostat (Leica CM1850; Leica Biosystem), and attached to microscope slides (Fisher Scientific). For staining of cultured neurons attached with SGCs, the samples were fixed with 4% PFA for 10 min at 4°C. The tissue and cultured cell samples were washed with PBS, blocked with 5% normal goat serum (Jackson ImmunoResearch) for 1 h at room temperature (RT) to prevent non-specific binding, and incubated overnight with the appropriate primary antibodies. The primary antibodies used are rabbit Kir4.1 (1:500, Alomone Labs), mouse Orai1 (1:200, Novus International), rabbit STIM1 (1:200, Cell Signaling Technology), and mouse glial fibrillary acidic protein (GFAP) (1:300, Santa Cruz Biotechnology). After washing with PBS, the samples were incubated with goat anti-rabbit/mouse AlexaFluor488 (1:400, Invitrogen) or goat anti-rabbit/-mouse AlexaFluor594 (1:400, Invitrogen) for 1 h at RT. After secondary antibody incubation, the samples were washed in PBS and counterstained for 5 min with 4,6-diamino-2-phenylindole dihydrochloride (1:1,000) (Sigma-Aldrich) to stain the nuclei. After washing out, the samples were mounted onto glass microscope slides with Vectashield antifade mounting medium (Vector Laboratories). For negative controls, all staining procedures were performed in the absence of primary antibodies. For hematoxylin and eosin (H&E) staining, paraffin-embedded ganglionic tissues were prepared and sectioned at 4 μm. The staining was performed at RT using 0.1% hematoxylin (Fisher Scientific) for 5 min and 0.4% eosin (Sigma-Aldrich) for

75 sec. Bright-field micrographs of H&E staining were captured using a 20× objective on an Olympus BX51 microscope (Olympus).

Image analysis

Confocal images including differential interference contrast images were acquired by using a Zeiss LSM800 confocal laser scanning microscope at high magnification (10× objective, NA 0.45; 20× objective, NA 0.8) controlled by ZEN2.3 software (Zeiss). For image processing and quantification of Orai1-positive puncta, the open-source software ImageJ (version 1.54; http:imagej.nih.gov/ij, National Institutes of Health) was used [22]. The background noises was removed using a Gaussian blur filter (sigma = 1). The images were made binary using the Otsu threshold method, and the puncta were counted using the "Analyze Particles" function in ImageJ.

Polymerase chain reaction (PCR) analysis

Total RNA was extracted from SCG using TRIzol Reagent (GeneAll Biotechnology). RNA quantity and purity were assessed using spectrophotometry. First-strand cDNA was synthesized from 500 ng of total RNA using ReverTra Ace qPCR Master Mix with gDNA Remover (Toyobo). RNA was denatured by heating to 65°C for 5 min and subsequent cDNA synthesis at 37°C for 15 min and 98°C for 5 min. Parallel reactions without reverse transcription were performed to confirm the absence of genomic DNA amplification. Using QuantStudio Real-Time PCR System (Applied Biosystems), SybrGreen-based real-time semi-quantitative PCR was initiated with an initial denaturation step of 96°C for 5 min, followed by 40 cycles of 96°C for 30 sec, 57°C for 30 sec, and 72°C for 2 min. The threshold cycle for each gene was determined and analyzed using the relative quantitation software. The relative expression of the target genes was calculated using the $2^{-\Delta\Delta CT}$ method. Parallel reactions without reverse transcription were performed to confirm the absence of genomic DNA amplification. The mRNA levels of the genes of interest were normalized to those of housekeeping gene GAPDH. Table 1 presents the primer sequences.

Immunoblot analysis

SCG were homogenized in RIPA Lysis and Extraction buffer (Thermo Fisher Scientific) supplemented with Halt Protease Inhibitor Cocktail (Fisher Scientific), and incubated for 20 min at 4°C. The lysates were centrifuged at 13,000 rpm for 20 min at 4°C to remove insoluble materials, the supernatant was collected for further experiments. Protein levels were quantified using the Bradford assay kit (Coomassie Protein Assay Reagent, Thermo Fisher Scientific). 80 μg of the sample was electrophoresed on an SDS-polyacrylamide gel (8%) and transferred onto a nitrocellulose (NC) membrane (Bio-Rad Laboratories). The membrane was blocked with 0.1% Tris-buffered saline/Tween-20 (TBST) containing 5% skim milk (Santa Cruz Biotechnology) for 1 h at RT and then incubated overnight at 4°C with primary antibodies against STIM1 (1:3,000), Orai1 (1:1,000), toll-like receptor 4 (TLR4) (1:1,000), GFAP (1:1,000), and GAPDH (1:10,000). After washing the primary antibodies with 0.1% TBST, the membranes were incubated with the secondary (1:2,000) goat anti-mouse or anti-rabbit IgG (H+L) secondary antibody, horseradish peroxidase-conjugated (Thermo Fisher Scientific) for 90 min at RT. After intense washing, immunoreactive bands were visualized on the NC membrane using an ECL detection reagent (GE Healthcare, no. RPN2235/2232) and Chemi Doc XRS+ imaging system (Bio-Rad Laboratories). The optical densities of the immunoreactive bands were quantified using the program Image Lab 5.2.1 (Bio-Rad Laboratories) and normalized to the loading control.

Measurement of intracellular Ca^{2+}

The partially dissociated cells on glass coverslips were loaded with 2.5 μM of Fura-2-acetoxymethyl ester (Fura-2 AM) (Thermo Fisher Scientific) for 45 min at 37°C in the culture medium, and subsequently washed with normal physiological salt solution (NPSS). The coverslips were then transferred to a perfusion chamber (Warner Instrument) on a TE2000 fluorescence microscope (Nikon) equipped with a ratio fluorescence system (RatioMaster; Photon Technology International Inc.). Cells were constantly perfused at 1 ml/min with an NPSS containing: NaCl 135 mM, KCl 4.5 mM, $MgCl_2$ 1 mM, $CaCl_2$ 2 mM, HEPES 10 mM, and glucose 10 mM (pH 7.4, 289–295 mOsm). Dye-loaded cells were alternatively excited at 340 and 380 nm, and the emitted light (510 nm) was captured after filtration using a CCD im-

Table 1. Sequences of primers used for quantitative PCR analysis

Gene	Primer sequences	Size product (bp)
GAPDH	F: CATCACTGCCACTCAGAAGACTG	153
	R: ATGCCAGTGAGCTTCCCGTTCAG	
Orai1	F: ACCGGGCACCCACTATGC	140
	R: ACTCTGCCCTGGTGAAGCCAG	
Orai2	F: TCCACCATCATCATGGTAC	162
	R: CACCTGTAGGCTTCTCTC	
Orai3	F: GCCCAGCTTTAGACTGTTGC	126
	R: CTGAGCAGGAATTTGGCTTC	
STIM1	F: ATGCCAATGGTGAATGTGGAT	97
	R: CCATGGAAGGTGCTGTGTTT	
STIM2	F: ACGGAAACCAAGAGCATG	199
	R: CGTGCGGGATGCTGCCTAC	
GFAP	F: CCAGATCCGAGAAACCAGCC	88
	R: CCGCATCTCCACCGTCTTTA	
TLR4	F: TCATGCTTTCTCACGGCCTC	142
	R: AGGAAGTACCTCTATGCAGGGAT	

F, forward; R, reverse.

aging instrument composed of Lambda DG-4 (Sutter Instrument Inc.) and CoolSNAP CCD (Cascade, Roper Scientific Inc.). Felix software for RatioMaster and Metafluor (V 6.1, Universal Imaging Corp.) for CoolSNAP CCD were used for data acquisition and analysis. The area under the curve (AUC) of the traces of Ca^{2+} changes during SOCE (AUC SOCE) was calculated for further comparative analysis.

Statistics

Statistical analyses were performed using Prism 10.0 (GraphPad Software). Comparisons were made using Student's t-test and one-way ANOVA with Tukey's *post-hoc* test. Statistical significance was set at $p < 0.05$ indicated as: *$p < 0.05$, **$p < 0.01$, ***$p < 0.001$. Data are presented as the mean ± SEM.

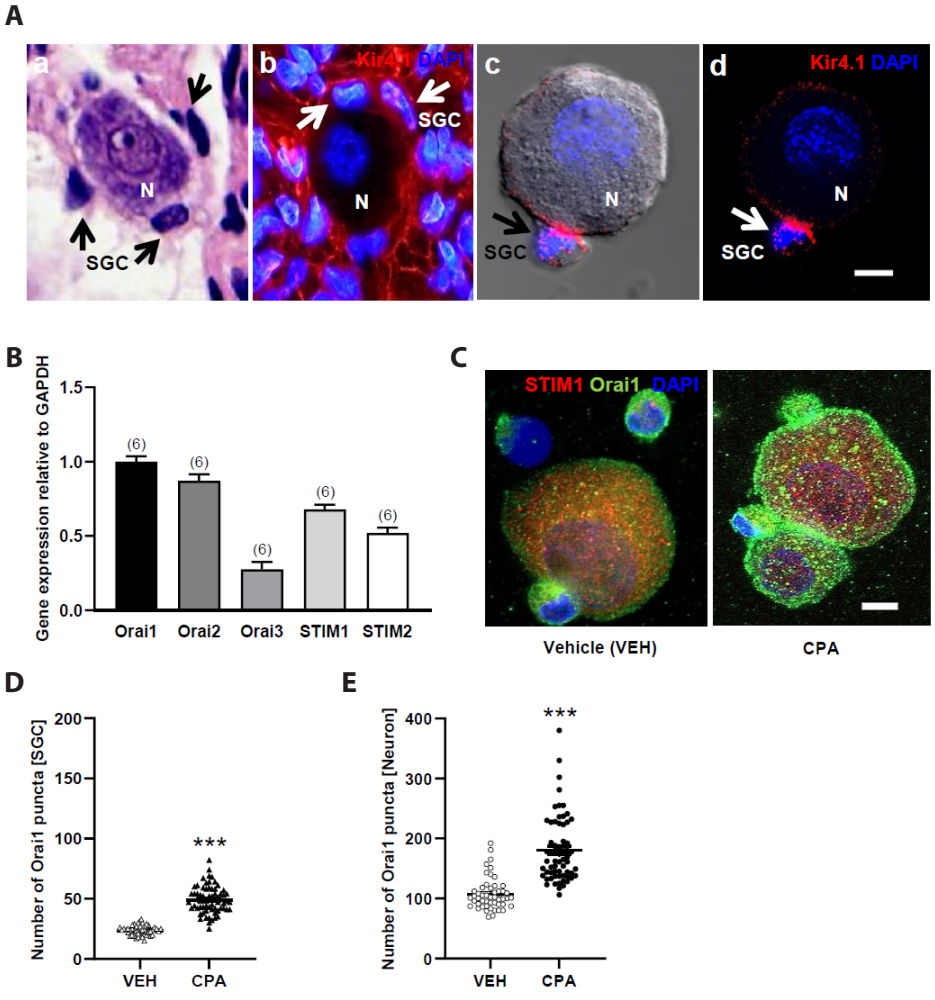

Fig. 1. Identification of the components of SOCE machinery in neurons and SGC units of rat sympathetic ganglia. (A, a) H&E staining to demonstrate the close localization of SGCs around the large soma of an SCG neuron. (A, b) Kir4.1-positive SGCs (arrows) enveloping SCG neurons (n). (A, c-d) DIC and immunofluorescent images of a neuron-SGC unit in the culture. SGCs showed Kir4.1-IR (arrow). DAPI was used to stain the nuclei of neuron and SGC. Scale bars = 10 μM. (B) Relative mRNA expressions of Orai and STIM, the SOCE components in sympathetic ganglia. The number of experiments is indicated in parentheses. (C) Representative immunofluorescent images of Orai1 (*green*) and STIM1 (*red*) distribution in a sympathetic neuron-SGC unit. DAPI was used to stain the nuclei of both neuron and SGC. Confocal images of the cells were captured before and after a 10-min treatment with 30 μM CPA. ER Ca^{2+} depletion with CPA induced the mobilization of STIM1-Orai1 aggregates, resulting in the assembly of prominent puncta formation in the cell surfaces of a neuron-SGC unit. Scale bars = 10 μM. (D, E). Summary of the number of Orai1 puncta in neuron-SGC units. Vehicle DMSO-treated (VEH) and CPA-treated (CPA) groups were compared (n = 54–60 cells from 5 wells per group). The data are presented as means ± SEM. Unpaired t-test, ***$p < 0.001$. SOCE, store-operated calcium entry; SGC, satellite glial cell; SCG, superior cervical ganglia; DIC, differential interference contrast; DAPI, 4,6-diamino-2-phenylindole dihydrochloride; STIM, stromal interaction molecule; CPA, cyclopiazonic acid; ER, endoplasmic reticulum; DMSO, dimethyl sulfoxide.

RESULTS

Identification of the components of SOCE machinery in the neurons and SGCs of rat sympathetic ganglia

H&E staining of a whole ganglia section revealed the morphologically unique location of SGCs around a large neuronal cell body (Fig. 1A, a). The previous studies have shown that the inwardly rectifying potassium channels Kir4.1 is an astrocyte and sensory SGCs-specific marker [23,24]. Recently, single-cell transcriptome analysis has revealed that the mRNAs encoding Kir4.1 are expressed in the SGCs of mouse SCG [4]. Consistent with these findings, we observed that the Kir4.1-positive SGCs closely envelop the large principal neurons in the rat sympathetic ganglia (Fig. 1A, b). For the *in vitro* simultaneous imaging of Ca^{2+} signaling in both neurons and SGCs, we used the method of partial enzymatic digestion with a BSA-gradient centrifugation process [21] for acquiring a pool of pure neuron-SGC units from sympathetic ganglia. We observed that a single SCG neuron was associated with one or more Kir4.1 expressing SGCs (Fig. 1A, c and 1A, d). Quantitative real-time PCR analysis showed that the transcripts encoding all known SOCE components (Orai1, Orai2, Orai3, STIM1, and STIM2) were expressed in rat SCG (Fig. 1B). Confocal images of immunofluorescence staining illustrated the presence of Orai1 and STIM1 in neurons and SGCs (Fig. 1C). When the ER Ca^{2+} store was depleted by 30 μM cyclopiazonic acid (CPA), an ER Ca^{2+} ATPase inhibitor, in the absence of extracellular Ca^{2+}, the Orai1- and STIM1-immunoreactivities were significantly increased on the plasma membranes of neurons and SGCs (Fig. 1C). The Orai1 channels were likely activated by the translocation and association of STIM1 [22]. We quantified the Orai1-immunoreactive puncta in neurons and SGCs. Compared with the control (vehicle [VEH]), CPA significantly increased the number of Orai1 puncta in neurons (Fig. 1D) and SGCs (Fig. 1E) ($p < 0.001$). On average, the number of Orai puncta before and after CPA treatment was 24 ± 1 (n = 50) and 49 ± 1 (n = 64), respectively in SGCs, and 107 ± 4 (n = 50) and 180 ± 7 (n = 64), respectively in neurons. These findings suggest that the SOCE machinery primarily comprises Orai1 and STIM1 in neurons and SGCs of the rat SCG.

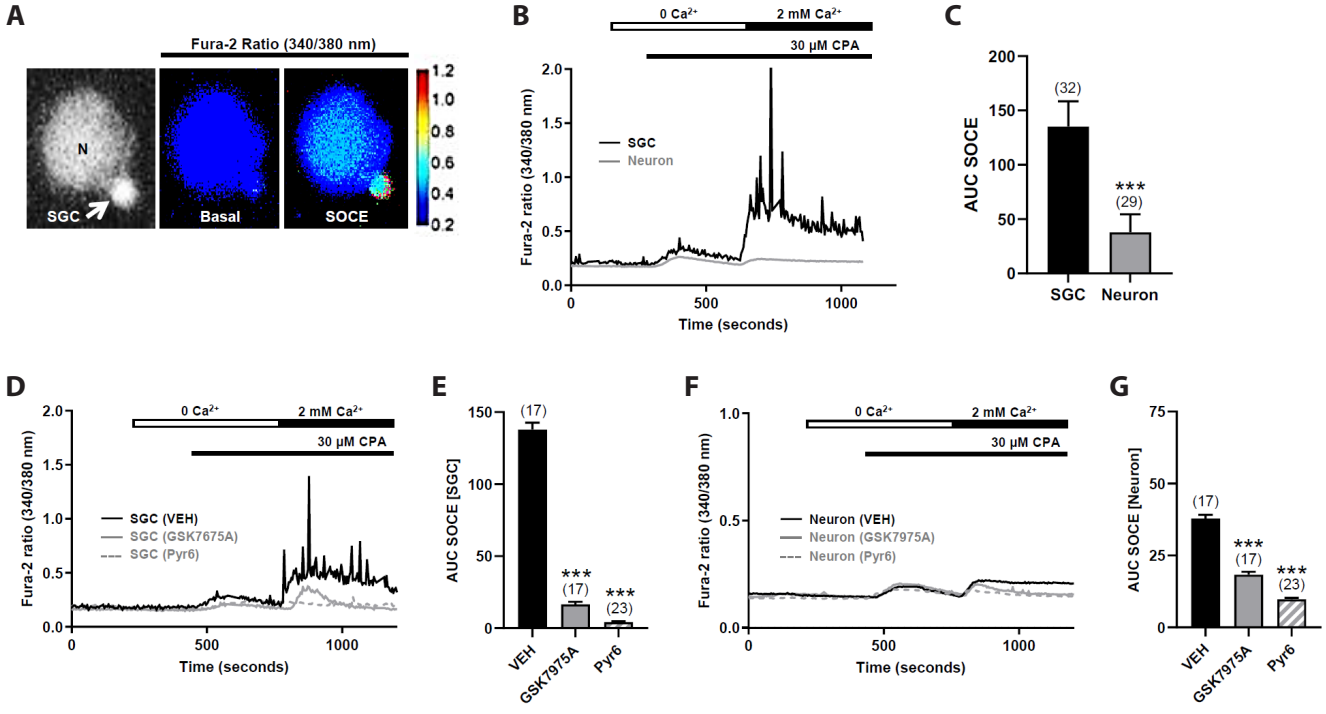

Fig. 2. Measurement of SOCE in both neurons and SGCs of sympathetic ganglia. (A) The digital images displaying a neuron-SGC unit (*left*), a 340 nm/380 nm ratio at the resting basal state (*middle*), and SOCE induction (*right*). (B) Representative traces of CPA (30 μM)-induced depletion of Ca^{2+} stores in the absence of external Ca^{2+} and the subsequent secondary Ca^{2+} influx (SOCE) *via* the activated CRAC by CPA in the presence of external Ca^{2+} (2 mM) in a neuron-SGC unit. The area under the curve (AUC) of the Ca^{2+} influx traces during SOCE, referred to AUC SOCE was measured in both SGCs and neurons. (C) Summary of AUC SOCE in both SGCs and neurons. Unpaired Student's t-test, ***$p < 0.001$. (D, F) Representative traces demonstrating pharmacological inhibition of SOCE with GSK7975A (1 μM for 1 h, Orai1 inhibitor) and Pyr6 (3 μM for 1 h, SOCE inhibitor) in a neuron-SGC unit. (E, G) Summary of AUC SOCE in both control (VEH) and inhibitor-treated SGCs and neurons. The data are presented as means ± SEM. The number of the tested cells is indicated in parentheses. One-way ANOVA followed by *post-hoc* Tukey's multiple comparison test, ***$p < 0.001$. SOCE, store-operated calcium entry; SGC, satellite glial cell; CPA, cyclopiazonic acid; CRAC, calcium release-activated calcium channel.

Measurement of SOCE in the neurons and SGCs of sympathetic ganglia

To ascertain whether SOCE proteins functional in sympathetic neurons and SGCs, we performed intracellular Ca^{2+} imaging experiments using Fura-2 AM. CPA-induced depletion of the ER Ca^{2+} store transiently increased the cytosolic Ca^{2+} level in the absence of extracellular Ca^{2+}. Subsequent perfusion of the buffer with 2 mM Ca^{2+} increased cytosolic Ca^{2+} in neurons and SGCs (Fig. 2A), suggesting that the store refilled Ca^{2+} influx *via* the activated SOCE channels (Fig. 2B). Interestingly, the magnitude of SOCE as measured in AUC SOCE (see Fig. 2B caption) was significantly larger in SGCs (135 ± 4, n = 32) than neurons (35 ± 3, n = 29) ($p < 0.001$) (Fig. 2C). It should be noted that the oscillating Ca^{2+} signals are likely a key feature of SOCE. We examined whether GSK7975A (1 μM), an Orai1/3 inhibitor, and Pyr6 (3 μM), an Orai1/TRPC3 inhibitor, suppressed CPA-induced SOCE. A previous study indicates that Pyr6 typically exhibits approximately 40-fold higher potency in inhibiting Orai1-mediated Ca^{2+} entry compared to TRPC3-mediated Ca^{2+} entry [25]. Accordingly, Pyr6 at 3 μM can selectively block orai1-mediated SOCE. After pre-treatment of these inhibitors for 1 h, SOCE was significantly suppressed in neurons and SGCs compared to the control (VEH) (Fig. 2D–G). On average, GSK7975A decreased the AUC SOCE by 88% in SGCs (138 ± 5 for control *vs*. 17 ± 2 for inhibitor, $p < 0.001$) (Fig. 2D, E) and 52% in neurons (38 ± 1 for control *vs*. 18 ± 1 for inhibitor, $p < 0.001$) (Fig. 2D, G). Pyr6 decreased the AUC SOCE by 97% in the SGCs (138 ± 5 for control *vs*. 4 ± 1 for inhibitor, $p < 0.001$) (Fig. 2E, F) and 74% in neurons (38 ± 1 for control *vs*. 10 ± 1 for inhibitor, $p < 0.001$) (Fig. 2F, G). These findings suggest that the SOCE machinery is functional in the neurons and SGCs of the rat sympathetic ganglia.

LPS decreased SOCE by downregulation of Orai1 and STIM1 expression in rat SCG

Next, we examined whether glial Ca^{2+} signaling is susceptible to pathological challenges. Acute systemic inflammation was induced in rats using LPS (2 mg/kg, intraperitoneal injection). One day after LPS injection, the expression of the transcripts encoding

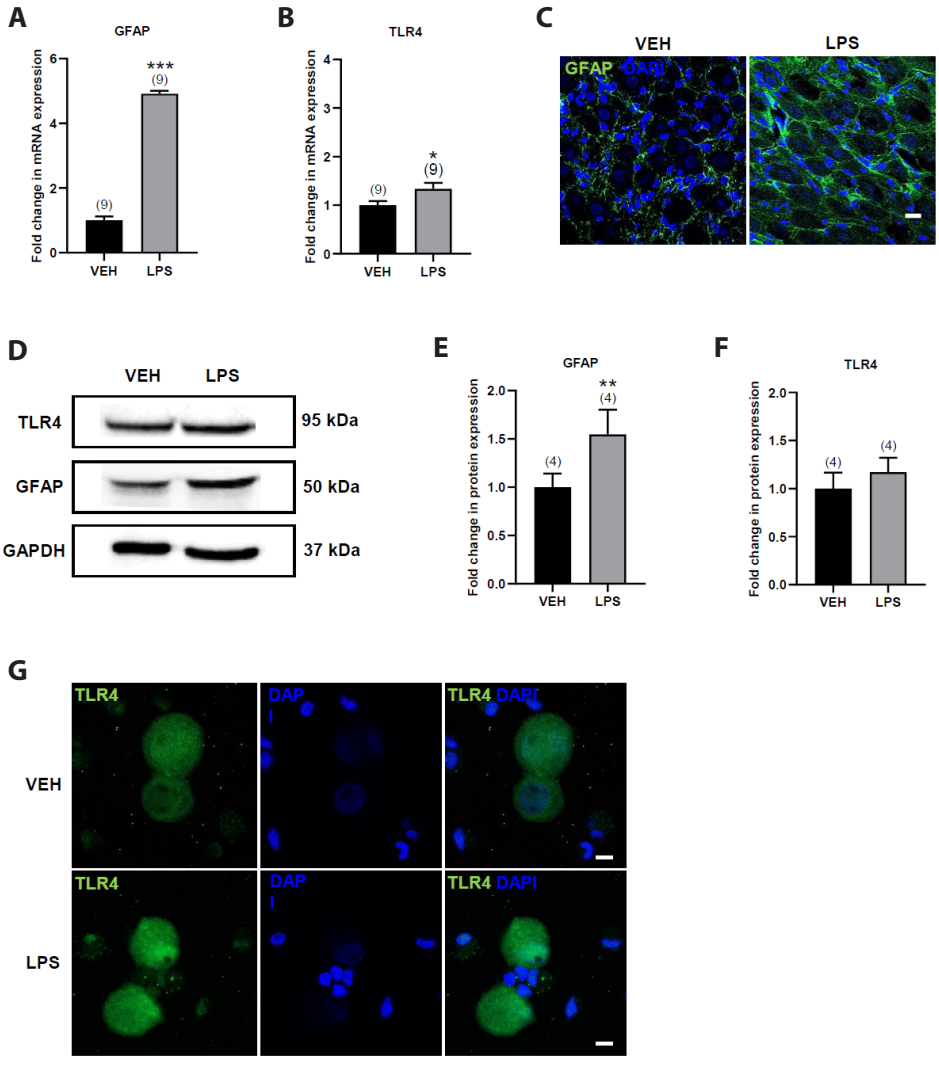

Fig. 3. LPS-induced upregulation of GFAP and TLR4 in sympathetic ganglia. (A, B) Real-time PCR analysis to assess the transcripts encoding GFAP and TLR4 in the sympathetic ganglia collected from rats with and without LPS injection (2 mg/kg, i.p., 24 h). (C) Confocal images depicting changes in GFAP expression in the SGCs of sympathetic ganglia 24 h after LPS injection. Scale bars = 10 μm. (D) Immunoblots of SCG collected from rats 24 h after injection of either vehicle or LPS *in vivo*. (E, F) Summary of the LPS-induced changes in the expression of GFAP and TLR4 proteins in the SCG. (G) Confocal images showing the localization and changes in TLR4 immunoreactivity in the control (VEH) and LPS (1 μg/ml, 24 h)-treated neuron-SGC units. Scale bars = 10 μm. Data are presented as means ± SEM. The number of experiments is indicated in parentheses. Unpaired Student's t-test, *$p < 0.05$, **$p < 0.01$, ***$p < 0.001$. LPS, lipopolysaccharide; GFAP, glial fibrillary acidic protein; TLR4, toll-like receptor 4; SGC, satellite glial cell; SCG, superior cervical ganglia; i.p., intraperitoneal; DAPI, 4,6-diamino-2-phenylindole dihydrochloride.

GFAP and TLR4, an LPS-responsive toll-like receptor, was upregulated approximately 4- and 1.4 folds, respectively, compared with that in the control (VEH) in the sympathetic ganglia ($p < 0.001$) (Fig. 3A, B). Immunohistochemical and immunoblotting analyses confirmed an LPS-mediated increase in GFAP expression (Fig. 3C–E). TLR4 protein levels increased slightly in the rat sympathetic ganglia (Fig. 3D, F). Next, we performed immunostaining of TLR4 in the cultured neurons and SGCs. As illustrated in Fig. 3G, TLR4 immunoactivity was prominently detected in neurons, while being negligible in individual SGCs under control (VEH) healthy conditions. Furthermore, 24 h following exposure to LPS (1 μg/ml) *in vitro*, TLR4 immunoactivity significantly increased in neurons. These findings suggest that LPS-induced reactive gliosis, *i.e*., the activation of SGCs, increases GFAP proteins in the SGCs *via* TLR4 activation in the rat sympathetic ganglia.

Importantly, the quantitative real-time PCR and immunoblotting analyses revealed that LPS significantly downregulated Orai1 and STIM1 expression in the rat sympathetic ganglia (Fig. 4A–D). We compared the SOCE in control and *in vitro* LPS (1 μg/ml for 24 h)-treated neurons and SGCs. LPS significantly decreased the magnitude of SOCE in SGCs and neurons (Fig. 4F–I). On average, LPS decreased the AUC SOCE by 41% in SGCs (153 ± 13 for VEH *vs*. 90 ± 15 for LPS, $p < 0.01$) (Fig. 4G) and 30% in neurons (Fig. 4I) (43 ± 4 for VEH *vs*. 30 ± 4 for LPS, $p < 0.05$). Finally, we examined whether LPS modulates Ca^{2+} influx through voltage-gated Ca^{2+} channels (VGCCs), the primary Ca^{2+} signaling pathway in neurons. Bath perfusion of high K^+ (80 mM) significantly increased the cytosolic Ca^{2+} levels in neurons (Supplementary Fig. 1A). In contrast, the individual SGCs in culture did not respond to high K^+ (data not shown) due to the absence of VGCCs. In a previous study, we found high K^+-induced Ca^{2+} signaling mediates somatic ATP release (unpublished data). Consequently, we observed ATP-mediated cytosolic Ca^{2+} increase in SGCs attached to neurons following high K^+ application (Supplementary Fig. 1C). Twenty-four hours after exposure to LPS (1 μg/ml), high K^+-induced cytosolic Ca^{2+} was significantly augmented in both neurons and SGCs attached to the attendant neurons. In summary, LPS increased the initial slope of cytosolic Ca^{2+} rise by 1.5- and 4.6-folds, respectively, in neurons and SGCs (Supplementary Fig. 1B, D). These findings suggested that LPS activates VGCC-mediated Ca^{2+} signaling, leading to an increase in somatic ATP release and, consequently, ATP-mediated Ca^{2+} signaling in SGCs of sympathetic ganglia.

DISCUSSION

In most electrically non-excitable cells, the depletion of ER Ca^{2+} store triggers secondary Ca^{2+} influx, known as SOCE, involving plasmalemmal channels [26]. Many studies have identified SOCE as the primary pathway for glial Ca^{2+} signaling in all types of glia within the central nervous system [27,28]. However, until

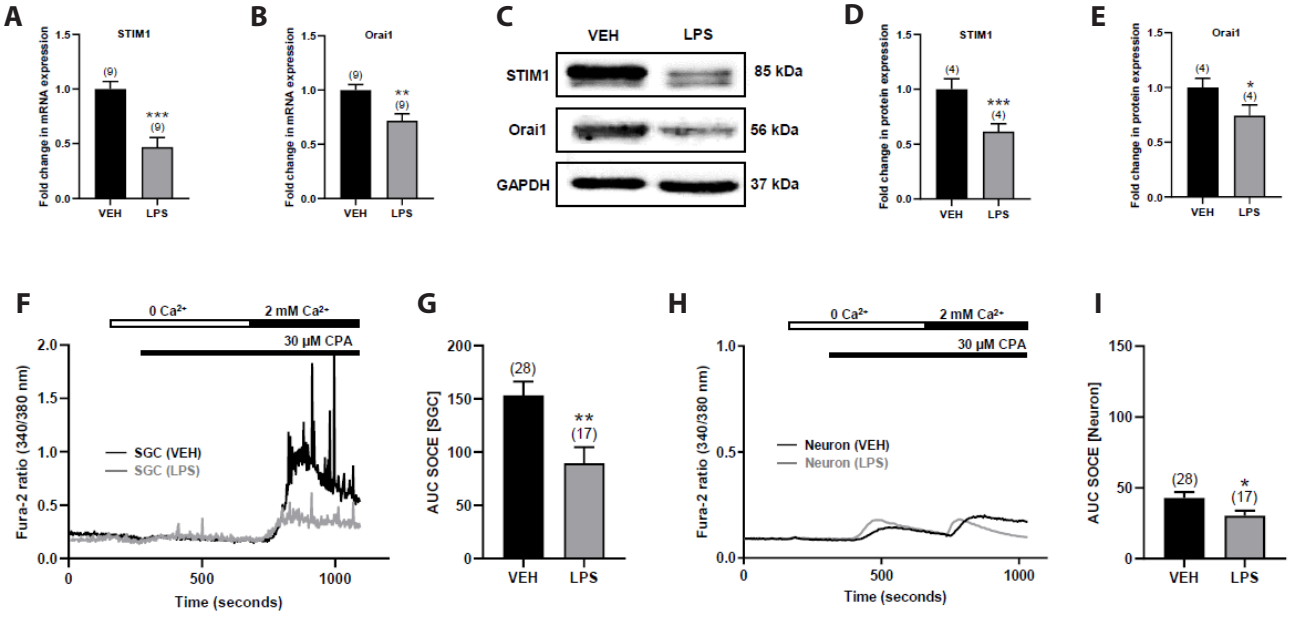

Fig. 4. LPS decreased SOCE by downregulating Orai 1 and STIM1 in the sympathetic ganglia. (A, B) Summary of the relative expression of transcripts encoding STIM1 and Orai1. (C) Immunoblots of Orai1 and STIM1 protein expression in rat SCG 24 h after either vehicle (VEH) or LPS injection *in vivo*. (D, E) Summary of the relative expression of Orai1 and STIM1 proteins. (F, H) Representative traces of SOCE in SGCs (F) and neurons (H) following treatment with either vehicle or LPS (1 μg/ml, 24 h *in vitro*). (G, I) Summary of the LPS-induced changes in AUC SOCE in both SGCs and neurons (n = 17–28 cells). The data are presented as means ± SEM. The number of experiments is indicated in parentheses. Unpaired Student's t-test, *$p < 0.05$, **$p < 0.01$, ***$p < 0.001$. LPS, lipopolysaccharide; SOCE, store-operated calcium entry; STIM, stromal interaction molecule; SCG, superior cervical ganglia; SGC, satellite glial cell; CPA, cyclopiazonic acid; AUC, area under the curve.

recently, little was known about the glial Ca^{2+} signaling mechanism in the peripheral nervous system including autonomic and sensory ganglia. Our investigation is the first time to reveal that sympathetic ganglia possess a functional SOCE machinery for glial Ca^{2+} signaling. The key findings of our study are as follows. First, the SOCE machinery in the sympathetic ganglia primarily comprises Orai1 and STIM1. Second, the depletion of the ER Ca^{2+} induced by CPA activates the SOCE machinery, allowing the secondary Ca^{2+} influx through plasmalemmal Orai channels. Thus, SOCE may play a more significant role in SGCs than in neurons. Third, LPS-induced inflammation down-regulates the expression of Orai1 and STIM1, consequently limiting SOCE.

The CRAC is one of the plasmalemmal channels responsible for mediating SOCE and comprises Orai (the plasmalemmal channel) and STIM (the ER Ca^{2+} sensor). Three Orai isoforms (Orai1-3), and two of STIM (STIM1 and STIM2) isoforms have been identified in vertebrates [29]. STIM1 and Orai1 are the central components of the SOCE machinery in numerous cell types, including astrocyte [30-34]. Our quantitative real-time PCR findings align with these discoveries, demonstrating the high expression of Orai1 and STIM1 in the sympathetic ganglia. Notably, we visually observed, for the first time, the transient organization of STIM1-Orai1 puncta induced by ER-Ca^{2+} depletion in the sympathetic ganglia. Additionally, the pharmacological inhibition of Orai1 significantly reduced the magnitude of SOCE. Our findings indicate that Orai1 and STIM1 are crucial in facilitating SOCE in sympathetic SGCs and neurons.

Cytoplasmic Ca^{2+} is an intracellular signal responsible for controlling many cellular processes. Ca^{2+} signaling in electrically excitable neurons mostly relies on the rapid and massive influx of Ca^{2+} *via* VGCCs, which are highly expressed on the plasma membranes. In contrast, non-electrically excitable SGCs do not express functional VGCCs and utilize ER Ca^{2+} store as the main source of cytoplasmic Ca^{2+} signaling [10,25,28]. Consequently, the SOCE machinery appears to be highly developed in SGCs in compared to neurons in the sympathetic ganglia.

Typically, in the glial cells, ER Ca^{2+} serve as the primary source of cytoplasmic Ca^{2+} signaling and predominantly mobilized *via* IP_3 receptor activation downstream of G-protein coupled receptor activation [35]. Various sources release diverse bioactive substances that potentially activate G-protein coupled receptors, including nerve terminals, neuronal cell bodies, glial cells. Recent studies have shown that acetylcholine (ACh) increases intracellular Ca^{2+} by engaging muscarinic receptors [36]. We observed that neuronal depolarization induces somatic ATP release through activation of VGCCs, which contributes to increased intracellular Ca^{2+}, partly through the activation of metabotropic purinergic receptor activation, specifically P2Y1 (unpublished data). Overall, ACh and ATP released from both preganglionic nerve terminals and postganglionic neuronal cell bodies are the principal mediators facilitating communication between neurons and SGCs. Hence, investigating whether the SOCE machinery (Orai1 and STIM1) is indispensable for muscarinic and purinergic receptors-mediated Ca^{2+} signaling could be an intriguing avenue for exploration.

A prominent feature of the SOCE in sympathetic SGCs is the presence of Ca^{2+} oscillations. Previous studies have suggested that the SOCE-related Ca^{2+} oscillations may originate from an intricate interplay between STIM1, transient receptor potential cation channels (TRPCs), and plasmalemmal and ER Ca^{2+} pumps [11,37]. Recently, we identified TRPC1, TRPC3, and TRPC6 in the sympathetic ganglia (unpublished data). Accordingly, we are exploring an alternative SOCE pathway that involves the interaction between STIM1 and TRPC channels in sympathetic SGCs.

SGCs are believed to influence various neural functions within the sympathetic ganglia [3]. Growing evidence has suggested that nerve injury and inflammation can modulate the functions of sensory SGCs, which are notably linked with pain sensation through TLR4 activation and GFAP upregulation-associated production of proinflammatory cytokines [2]. Recent studies have remarkably demonstrated that LPS-induced upregulation of SOCE increases proinflammatory cytokine production in spinal astrocytes, and initiates inflammatory signaling pathways in a mouse hippocampal cell line [19,38]. In contrast, we found that LPS diminished SOCE by downregulating Orai1 and STIM1 expression in the sympathetic ganglia. LPS-induced downregulation of SOCE has been consistently reported in different glial cell types, including hippocampal astrocytes and microglia [14,17,39]. We are currently uncertain about the source of the discrepancy in LPS-induced regulation of SOCE. Future research on the signaling mechanisms underlying the LPS-induced downregulation of SOCE machinery in rat sympathetic ganglia is awaited.

The upregulation of GFAP is a widely used hallmark of glial activation and reactive gliosis [40]. Hanani group [41] demonstrated that LPS upregulates GFAP expression through TLR4 activation in mouse trigeminal ganglia. They also suggested that the absence of TLR4 in mouse SCG prevents reactive gliosis in response to LPS exposure. In contrast, we observed that TLR4 is expressed in rat sympathetic ganglia, and mediates the activation of SGCs in response to LPS exposure. A previous study has shown that sciatic nerve injury causes GFAP upregulation in the sensory ganglia of rats, but not in mice [42]. There appear to be differences in how species respond to certain pathological conditions.

TLR4 mediates the production of proinflammatory cytokines such as tumor necrosis factor-alpha and interleukin 1 beta in neurons, astrocytes, and microglia [43,44]. Unexpectedly, our immunocytochemical staining of the neuron-SGC units demonstrated that SCG neurons, but not SGCs, highly expressed TLR4, suggesting that neurons are the major cellular sources of proinflammatory cytokines in the rat SCG. In general, the release of proinflammatory cytokines is regulated by Ca^{2+}-dependent signaling mechanisms that activate several transcription factor pathways, including nuclear factor kappa B, NFAT, and cAMP response element-binding protein [45-47]. In SCG neurons, it is unlikely that SOCE mediates the release of proinflammatory

cytokines due to the LPS-induced downregulation of Orai1 and STIM1. In contrast, LPS increased Ca^{2+} influx through VGCCs (Supplementary Fig. 1), suggesting an alternative mechanism for the Ca^{2+}-dependent release of proinflammatory cytokines induced in SCG neurons. VGCCs in sympathetic neurons comprise N, L, and R types [48]. Evidence supports that STIM1 can trigger the internalization of L-type Cav1.2 channels from the plasma membrane through physical binding in multiple cell types, including neurons and vascular smooth muscle [49,50]. A recent study showed that loss of STIM1 potentiates Ca^{2+} entry through Cav1.2, resulting in cell death [51]. Consequently, we speculate that the LPS-induced increase in Ca^{2+} entry through VGCCs is associated with the potentiation of Cav1.2 due to reduced STM1 expression in rat SCG neurons.

SGCs in the peripheral ganglia have immune properties and expressing mitogen-activated protein kinases and cytokines [52,53]. Consequently, we consider that, in addition to neurons, SGCs can release proinflammatory cytokines through alternative pathways, even though their expression of TLR4, if any, is weak. As mentioned previously, SOCE is the primary Ca^{2+} signaling mechanism in sympathetic SGCs. An alternative Ca^{2+} signaling pathway might involve Ca^{2+} influx across the plasma membrane *via* ion channels such as P2X receptors. Among the known P2X receptor isoforms, P2X7 mediates LPS-induced inflammation [54]. On the other hand, interleukin 1 beta upregulates P2X7 expression in human astrocytes [55]. We observed that P2X7 was expressed together with P2Y in healthy sympathetic SGCs. Overall, it might be worth examining whether LPS-induced activation of somatic ATP and cytokine release occurs through STIM1 downregulation-mediated activation of Cav1.2, and increase SGC Ca^{2+} signaling by activating the upregulated P2X7 in the sympathetic ganglia.

In conclusion, our findings offer foundational insights into the major mechanism of Ca^{2+} signaling in SGCs, comparing them with the principal neurons in the sympathetic ganglia. Emerging evidence support the new hypothesis indicating that the complex network contributing to final visceral motor output involves neurons and glial cells within the autonomic ganglia. For instance, activating Gq G protein-coupled receptors in sympathetic SGCs significantly accelerates cardiovascular functions [56]. This observation suggests that maintaining glial Ca^{2+} homeostasis is critical for neural activity in the sympathetic ganglia. Several pathological conditions including chronic heart failure [5], liver cirrhosis [6], and traumatic brain injury [7], lead to autonomic imbalance characterized by sympathetic overactivity. Thus, whether dysregulation of SOCE contributes to alterations in sympathetic output during these diseased states remains to be explored.

FUNDING

This research was supported by Basic Science Research Program through the National Research Foundation funded by the Ministry of Education, Science and Technology (NRF-2016 R1 D1A1B01015042).

ACKNOWLEDGEMENT

We thank Professors Kyu-Sang Park and Seung-Kuy Cha for proofreading this manuscript.

CONFLICTS OF INTEREST

The authors declare no conflicts of interest.

SUPPLEMENTARY MATERIALS

Supplementary data including one figure can be found with this article online at https://doi.org/10.4196/kjpp.2024.28.1.93

REFERENCES

1. Hanani M. Satellite glial cells in sympathetic and parasympathetic ganglia: in search of function. *Brain Res Rev.* 2010;64:304-327.
2. Hanani M, Spray DC. Emerging importance of satellite glia in nervous system function and dysfunction. *Nat Rev Neurosci.* 2020;21:485-498. Erratum in: *Nat Rev Neurosci.* 2020;21:732.
3. Enes J, Haburčák M, Sona S, Gerard N, Mitchell AC, Fu W, Birren SJ. Satellite glial cells modulate cholinergic transmission between sympathetic neurons. *PLoS One.* 2020;15:e0218643.
4. Mapps AA, Boehm E, Beier C, Keenan WT, Langel J, Liu M, Thomsen MB, Hattar S, Zhao H, Tampakakis E, Kuruvilla R. Satellite glia modulate sympathetic neuron survival, activity, and autonomic function. *Elife*. 2022;11:e74295.
5. Tu H, Liu J, Zhu Z, Zhang L, Pipinos II, Li YL. Mitochondria-derived superoxide and voltage-gated sodium channels in baroreceptor neurons from chronic heart-failure rats. *J Neurophysiol*. 2012;107:591-602.
6. Lee CK, Park KH, Baik SK, Jeong SW. Decreased excitability and voltage-gated sodium currents in aortic baroreceptor neurons contribute to the impairment of arterial baroreflex in cirrhotic rats. *Am J Physiol Regul Integr Comp Physiol.* 2016;310:R1088-R1101.
7. Oh JW, Lee CK, Whang K, Jeong SW. Functional plasticity of cardiac efferent neurons contributes to traumatic brain injury-induced cardiac autonomic dysfunction. *Brain Res*. 2021;1753:147257.
8. Araque A. Astrocytes process synaptic information. *Neuron Glia Biol*. 2008;4:3-10.
9. Verkhratsky A, Nedergaard M. Physiology of astroglia. *Physiol Rev.* 2018;98:239-389.
10. Perea G, Araque A. Glial calcium signaling and neuron-glia communication. *Cell Calcium*. 2005;38:375-382.
11. Prakriya M, Lewis RS. Store-operated calcium channels. *Physiol Rev.* 2015;95:1383-1436.

12. Verkhratsky A, Parpura V. Astrogliopathology in neurological, neurodevelopmental and psychiatric disorders. *Neurobiol Dis.* 2016;85:254-261.
13. Guner G, Guzelsoy G, Isleyen FS, Sahin GS, Akkaya C, Bayam E, Kotan EI, Kabakcioglu A, Ince-Dunn G. NEUROD2 regulates *Stim1* expression and store-operated calcium entry in cortical neurons. *eNeuro.* 2017;4:ENEURO.0255-16.2017.
14. Heo DK, Lim HM, Nam JH, Lee MG, Kim JY. Regulation of phagocytosis and cytokine secretion by store-operated calcium entry in primary isolated murine microglia. *Cell Signal*. 2015;27:177-186.
15. Korkotian E, Oni-Biton E, Segal M. The role of the store-operated calcium entry channel Orai1 in cultured rat hippocampal synapse formation and plasticity. *J Physiol*. 2017;595:125-140.
16. Molnár T, Yarishkin O, Iuso A, Barabas P, Jones B, Marc RE, Phuong TT, Križaj D. Store-operated calcium entry in Müller glia is controlled by synergistic activation of TRPC and Orai channels. *J Neurosci*. 2016;36:3184-3198.
17. Pereira OR Jr, Ramos VM, Cabral-Costa JV, Kowaltowski AJ. Changes in mitochondrial morphology modulate LPS-induced loss of calcium homeostasis in BV-2 microglial cells. *J Bioenerg Biomembr*. 2021;53:109-118.
18. Toth AB, Hori K, Novakovic MM, Bernstein NG, Lambot L, Prakriya M. CRAC channels regulate astrocyte Ca^{2+} signaling and gliotransmitter release to modulate hippocampal GABAergic transmission. *Sci Signal*. 2019;12:eaaw5450.
19. Birla H, Xia J, Gao X, Zhao H, Wang F, Patel S, Amponsah A, Bekker A, Tao YX, Hu H. Toll-like receptor 4 activation enhances Orai1-mediated calcium signal promoting cytokine production in spinal astrocytes. *Cell Calcium*. 2022;105:102619.
20. Ikeda SR, Jeong SW. Use of RGS-insensitive Galpha subunits to study endogenous RGS protein action on G-protein modulation of N-type calcium channels in sympathetic neurons. *Methods Enzymol*. 2004;389:170-189.
21. George D, Ahrens P, Lambert S. Satellite glial cells represent a population of developmentally arrested Schwann cells. *Glia*. 2018;66:1496-1506.
22. Buijs TJ, Vilar B, Tan CH, McNaughton PA. STIM1 and ORAI1 form a novel cold transduction mechanism in sensory and sympathetic neurons. *EMBO J*. 2023;42:e111348.
23. Butt AM, Kalsi A. Inwardly rectifying potassium channels (Kir) in central nervous system glia: a special role for Kir4.1 in glial functions. *J Cell Mol Med*. 2006;10:33-44.
24. Tang X, Schmidt TM, Perez-Leighton CE, Kofuji P. Inwardly rectifying potassium channel Kir4.1 is responsible for the native inward potassium conductance of satellite glial cells in sensory ganglia. *Neuroscience.* 2010;166:397-407.
25. Schleifer H, Doleschal B, Lichtenegger M, Oppenrieder R, Derler I, Frischauf I, Glasnov TN, Kappe CO, Romanin C, Groschner K. Novel pyrazole compounds for pharmacological discrimination between receptor-operated and store-operated Ca(2+) entry pathways. *Br J Pharmacol*. 2012;167:1712-1722.
26. Verkhratsky A, Rodríguez JJ, Parpura V. Calcium signalling in astroglia. *Mol Cell Endocrinol.* 2012;353:45-56.
27. Pivneva T, Haas B, Reyes-Haro D, Laube G, Veh RW, Nolte C, Skibo G, Kettenmann H. Store-operated Ca2+ entry in astrocytes: different spatial arrangement of endoplasmic reticulum explains functional diversity in vitro and in situ. *Cell Calcium*. 2008;43:591-601.
28. Lo KJ, Luk HN, Chin TY, Chueh SH. Store depletion-induced calcium influx in rat cerebellar astrocytes. *Br J Pharmacol*. 2002;135:1383-1392.
29. Verkhratsky A, Parpura V. Store-operated calcium entry in neuroglia. *Neurosci Bull*. 2014;30:125-133.
30. Roos J, DiGregorio PJ, Yeromin AV, Ohlsen K, Lioudyno M, Zhang S, Safrina O, Kozak JA, Wagner SL, Cahalan MD, Veliçelebi G, Stauderman KA. STIM1, an essential and conserved component of store-operated Ca2+ channel function. *J Cell Biol*. 2005;169:435-445.
31. Prakriya M, Feske S, Gwack Y, Srikanth S, Rao A, Hogan PG. Orai1 is an essential pore subunit of the CRAC channel. *Nature*. 2006;443:230-233.
32. Moreno C, Sampieri A, Vivas O, Peña-Segura C, Vaca L. STIM1 and Orai1 mediate thrombin-induced Ca(2+) influx in rat cortical astrocytes. *Cell Calcium*. 2012;52:457-467.
33. Liou J, Kim ML, Heo WD, Jones JT, Myers JW, Ferrell JE Jr, Meyer T. STIM is a Ca2+ sensor essential for Ca2+-store-depletion-triggered Ca2+ influx. *Curr Biol*. 2005;15:1235-1241.
34. Feske S, Gwack Y, Prakriya M, Srikanth S, Puppel SH, Tanasa B, Hogan PG, Lewis RS, Daly M, Rao A. A mutation in Orai1 causes immune deficiency by abrogating CRAC channel function. *Nature*. 2006;441:179-185.
35. Alberdi E, Sánchez-Gómez MV, Matute C. Calcium and glial cell death. *Cell Calcium*. 2005;38:417-425.
36. Feldman-Goriachnik R, Wu B, Hanani M. Cholinergic responses of satellite glial cells in the superior cervical ganglia. *Neurosci Lett*. 2018;671:19-24.
37. Putney JW Jr. A model for receptor-regulated calcium entry. *Cell Calcium*. 1986;7:1-12.
38. Sun Z, Li X, Yang L, Dong X, Han Y, Li Y, Luo J, Li W. SOCE-mediated NFAT1-NOX2-NLRP1 inflammasome involves in lipopolysaccharide-induced neuronal damage and Aβ generation. *Mol Neurobiol.* 2022;59:3183-3205.
39. Ronco V, Grolla AA, Glasnov TN, Canonico PL, Verkhratsky A, Genazzani AA, Lim D. Differential deregulation of astrocytic calcium signalling by amyloid-β, TNFα, IL-1β and LPS. *Cell Calcium*. 2014;55:219-229.
40. Liddelow SA, Barres BA. Reactive astrocytes: production, function, and therapeutic potential. *Immunity*. 2017;46:957-967.
41. Feldman-Goriachnik R, Hanani M. The effects of sympathetic nerve damage on satellite glial cells in the mouse superior cervical ganglion. *Auton Neurosci*. 2019;221:102584.
42. Mohr KM, Pallesen LT, Richner M, Vaegter CB. Discrepancy in the usage of GFAP as a marker of satellite glial cell reactivity. *Biomedicines*. 2021;9:1022.
43. Campolo M, Paterniti I, Siracusa R, Filippone A, Esposito E, Cuzzocrea S. TLR4 absence reduces neuroinflammation and inflammasome activation in Parkinson's diseases in vivo model. *Brain Behav Immun*. 2019;76:236-247.
44. Bruno K, Woller SA, Miller YI, Yaksh TL, Wallace M, Beaton G, Chakravarthy K. Targeting toll-like receptor-4 (TLR4)-an emerging therapeutic target for persistent pain states. *Pain*. 2018;159:1908-1915.
45. Vuong B, Hogan-Cann AD, Alano CC, Stevenson M, Chan WY, Anderson CM, Swanson RA, Kauppinen TM. NF-κB transcriptional activation by TNFα requires phospholipase C, extracellular signal-regulated kinase 2 and poly(ADP-ribose) polymerase-1. *J*

Neuroinflammation. 2015;12:229.
46. Pulver RA, Rose-Curtis P, Roe MW, Wellman GC, Lounsbury KM. Store-operated Ca2+ entry activates the CREB transcription factor in vascular smooth muscle. *Circ Res*. 2004;94:1351-1358.
47. Crabtree GR, Olson EN. NFAT signaling: choreographing the social lives of cells. *Cell.* 2002;109 Suppl:S67-S79.
48. Won YJ, Whang K, Kong ID, Park KS, Lee JW, Jeong SW. Expression profiles of high voltage-activated calcium channels in sympathetic and parasympathetic pelvic ganglion neurons innervating the urogenital system. *J Pharmacol Exp Ther*. 2006;317:1064-1071.
49. Park CY, Shcheglovitov A, Dolmetsch R. The CRAC channel activator STIM1 binds and inhibits L-type voltage-gated calcium channels. *Science*. 2010;330:101-105.
50. Wang Y, Deng X, Mancarella S, Hendron E, Eguchi S, Soboloff J, Tang XD, Gill DL. The calcium store sensor, STIM1, reciprocally controls Orai and CaV1.2 channels. *Science*. 2010;330:105-109.
51. Pascual-Caro C, Berrocal M, Lopez-Guerrero AM, Alvarez-Barrientos A, Pozo-Guisado E, Gutierrez-Merino C, Mata AM, Martin-Romero FJ. STIM1 deficiency is linked to Alzheimer's disease and triggers cell death in SH-SY5Y cells by upregulation of L-type voltage-operated Ca^{2+} entry. *J Mol Med (Berl).* 2018;96:1061-1079. Erratum in: *J Mol Med (Berl).* 2019;97:1215-1217.
52. Afroz S, Arakaki R, Iwasa T, Oshima M, Hosoki M, Inoue M, Baba O, Okayama Y, Matsuka Y. CGRP induces differential regulation of cytokines from satellite glial cells in trigeminal ganglia and orofacial nociception. *Int J Mol Sci*. 2019;20:711.
53. Vause CV, Durham PL. Calcitonin gene-related peptide differentially regulates gene and protein expression in trigeminal glia cells: findings from array analysis. *Neurosci Lett*. 2010;473:163-167.
54. Ren WJ, Illes P. Involvement of P2X7 receptors in chronic pain disorders. *Purinergic Signal*. 2022;18:83-92.
55. Narcisse L, Scemes E, Zhao Y, Lee SC, Brosnan CF. The cytokine IL-1beta transiently enhances P2X7 receptor expression and function in human astrocytes. *Glia*. 2005;49:245-258.
56. Xie AX, Lee JJ, McCarthy KD. Ganglionic $GFAP^{+}$ glial Gq-GPCR signaling enhances heart functions in vivo. *JCI Insight*. 2017; 2:e90565.